Published in final edited form as:

Hepatology. 2021 October ; 74(4): 1845–1863. doi:10.1002/hep.31871.

Inhibition of secretin/secretin receptor axis ameliorates non-alcoholic fatty liver disease phenotypes

Lixian Chen[1,#], **Nan Wu**[1,#], **Lindsey Kennedy**[1], **Heather Francis**[1,2], **Ludovica Ceci**[1], **Tianhao Zhou**[1], **Niharika Samala**[1], **Konstantina Kyritsi**[1], **Chaodong Wu**[4], **Amelia Sybenga**[5], **Burcin Ekser**[6], **Wasim Dar**[7], **Constance Atkins**[8], **Vik Meadows**[1], **Shannon Glaser**[3,*], **Gianfranco Alpini**[1,2,*]

[1]Division of Gastroenterology and Hepatology, Department of Medicine, Indiana University, Indianapolis, IN

[2]Richard L. Roudebush VA Medical Center, Indianapolis, IN

[3]Department of Medical Physiology, Texas A&M University, College of Medicine, Bryan, TX

[4]Department of Nutrition, Texas A&M University, College Station, TX

[5]Department of Pathology, Laboratory Medicine, University of Vermont Medical Center, Burlington, VT

[6]Division of Transplant Surgery, Department of Surgery, Indiana University School of Medicine, Indianapolis, IN

[7]Department of Surgery, Division of Acute Care Surgery, The University of Texas Health Sciences Center at Houston

[8]Department of Anesthesiology, University of Texas Health Sciences Center at Houston

Abstract

Background & Aims: Human non-alcoholic fatty liver disease (NAFLD) is characterized at early stages by hepatic steatosis, which may progress to nonalcoholic steatohepatitis (NASH) when the liver displays microvesicular steatosis, lobular inflammation, and pericellular fibrosis. The secretin (SCT)/secretin receptor (SCTR) axis promotes biliary senescence and liver fibrosis in cholestatic models through downregulation of miR-125b signaling. We aim to evaluate the effect of disrupting biliary SCT/SCTR/miR-125b signaling on hepatic steatosis, biliary senescence and liver fibrosis in NAFLD/NASH.

Approach & Results: *In vivo,* 4 wk male WT, *Sct*$^{-/-}$ and *Sctr*$^{-/-}$ mice were fed a control diet (CD) or high-fat diet (HFD) for 16 wks. The expression of SCT/SCTR/miR-125b axis was measured in human NAFLD/NASH liver samples and HFD mouse livers by

Address correspondence to: Gianfranco Alpini, Ph.D., Professor of Medicine, VA Senior Research Scientist, Hickam Endowed Chair, Director, Indiana Center for Liver Research, Richard L. Roudebush VA Medical Center and Indiana University, Gastroenterology, Medicine, 1481 W 10th street, Dedication Wing – Room D-2004, Indianapolis, IN 46202, galpini@iu.edu or Gianfranco.alpini@va.gov.

[#]Drs. Chen and Wu share the first authorship

[*]Drs. Glaser and Alpini share the senior authorship

Conflict of interest statement: The authors have declared that no conflict of interest exists.

immunohistochemistry (IHC) and *q*PCR. Biliary/hepatocyte senescence, ductular reaction and liver angiogenesis were evaluated in mouse liver and human NAFLD/NASH liver samples. miR-125b target lipogenesis genes in hepatocytes were screened and validated by custom RT^2 Profiler PCR array and luciferase assay. Biliary SCT/SCTR expression was increased in human NAFLD/NASH samples and in livers of HFD mice, whereas the expression of miR-125b was decreased. Biliary/hepatocyte senescence, ductular reaction, and liver angiogenesis were observed in human NAFLD/NASH samples as well as HFD mice, which were decreased in *Sct*$^{-/-}$ and *Sctr*$^{-/-}$ HFD mice. *Elovl1* is a lipogenesis gene targeted by miR-125b, and its expression was also decreased in HFD mouse hepatocytes following *Sct* or *Sctr* knockout. Bile acid profile in fecal samples have the greatest changes between WT mice and *Sct*$^{-/-}$/*Sctr*$^{-/-}$ mice.

Conclusion: The biliary SCT/SCTR/miR-125b axis promotes liver steatosis by upregulating lipid biosynthesis gene *Elovl1*. Targeting the biliary SCT/SCTR/miR-125b axis may be key for ameliorating phenotypes of human NAFLD/NASH.

Keywords

hepatic steatosis; miR-125b; ELOVL1; ductular reaction; angiogenesis

Introduction

Nonalcoholic fatty liver disease (NAFLD), characterized by hepatic steatosis, is an alarming public health concern and is considered the most common liver disease worldwide (1). Simple steatosis can progress to nonalcoholic steatohepatitis (NASH) when the liver displays microvesicular steatosis, hepatocellular ballooning, lobular inflammation and pericellular fibrosis (2). NASH is a growing cause of liver cirrhosis and hepatocellular carcinoma ultimately leading to liver failure (3).

During cholestasis, cholangiocytes are the key link between biliary damage and fibrosis that characterizes chronic hepatobiliary injury, through the products of their activation like secretin (SCT) (4–6). Recent evidence indicates that cholangiocytes play a role in the pathogenesis of NAFLD through activation of biliary proliferation (ductular reaction, DR) and subsequent liver fibrosis (7, 8). One study found that secretin receptor (SCTR) knockout mice are resistant to high-fat diet (HFD)-induced obesity and exhibit impaired intestinal lipid absorption (9); however, the role of the SCT/SCTR axis in NAFLD/NASH progression remains unknown.

Liver steatosis is determined by *de novo* lipogenesis, lipid uptake, fatty acid β-oxidation, and very low-density lipoprotein (VLDL) secretion (10). Lipogenesis is regulated by acetyl-CoA being converted to malonyl-CoA by acetyl-CoA carboxylase (ACC), and malonyl-CoA is then converted to palmitate by fatty acid synthase (FASN) (11). Elevated lipogenesis, in combination with excess adipose fatty acid release, is a significant contributor to NAFLD (12). Elongation of very-long-chain fatty acids 1 (ELOVL1) is key for the synthesis of Cer d24:0 and Cer d24:1(13); however, the relevance of ELOVL1 in NAFLD and NASH remains unknown.

miRNAs, which are small non-coding RNAs that regulate gene expression via RNA silencing and post-transcriptional modification, may regulate lipid metabolism in the liver (14, 15). The SCT/SCTR axis stimulates biliary senescence and liver fibrosis during cholestasis by downregulation of miR-125b (6). miR-125b inhibits fat accumulation in the liver during HFD (16) and regulates vascular endothelial growth factor-A (VEGF-A) expression during cholestasis (17). Liver angiogenesis increases in NAFLD and contributes to inflammation, fibrosis, and hepatocellular carcinoma development (18). The present study was conducted using a HFD fed mouse model, as well as human NAFLD and NASH samples to evaluate the role of the SCT/SCTR/miR-125b axis in NAFLD, and to explore the potential target lipogenesis genes of miR-125b.

Materials and methods

Materials

Reagents were purchased from Sigma-Aldrich (St. Louis, MO) unless otherwise indicated. The antibodies for SCT and SCTR were obtained from Bioss (Woburn, MA) and Abcam (Cambridge, MA). The antibodies for cytokeratin-19 (CK-19), desmin, cyclin-dependent kinase inhibitor 2A (p16), VEGF-A, cluster of differentiation 68 (CD68) and von Willebrand factor (vWF) were obtained from Abcam (Cambridge, MA). Cluster of differentiation 31 (CD31) antibody was purchased from R&D (Minneapolis, MN). The monoclonal antibody for F4/80 was purchased from Cell Signaling Technology (Danvers, MA). The two different antibodies for ELOVL1 were purchased from both Thermo Fisher Scientific (Mountain View, CA) and Abcam (Cambridge, MA). Commercially available enzyme-linked immunosorbent assay (ELISA) kits for measuring SCT levels were purchased from Phoenix Pharmaceuticals (Burlingame, CA). ELISA kits to measure transforming growth factor-β1 (TGF-β1) levels in serum and cholangiocyte supernatant were purchased from Abcam. The mirVana™ miRNA Isolation Kit for RNA isolation was purchased from Ambion (Mountain View, CA). Selected mouse and human PCR primers were purchased from Qiagen (Valencia, CA). The iScript cDNA Synthesis Kit (170–8891) and iTaq Universal SYBR Green Supermix were purchased from Bio-Rad (Hercules, CA). The information on real-time PCR (*q*PCR) primers used is listed in the Supplemental Table 1.

Animal models

Animal procedures were performed according to protocols approved by the Baylor Scott & White Health and Indiana University School of Medicine Institutional Animal Care and Use Committees. C57/BL6 wild-type (WT) mice were purchased from Charles River (Wilmington, MA). *Sct*$^{-/-}$ and *Sctr*$^{-/-}$ mouse colonies are established in our facility (19); mice were originally obtained from Billy K. C. Chow, School of Biological Sciences, The University of Hong Kong, Hong Kong. *Sctr*$^{-/-}$ mice did not differ in locomotor activity or energy expenditure compared with WT mice (9). We did not observe any specific hepatic phenotypes in *Sct*$^{-/-}$ and *Sctr*$^{-/-}$ compared to WT mice. Mice were maintained in microisolator cages in a temperature-controlled environment with 12:12-hour light-dark cycles. Studies were performed in 4-week old male WT, *Sct*$^{-/-}$ and *Sctr*$^{-/-}$ mice fed either a control diet (CD, Envigo, Indianapolis, IN) consisting of standard chow and reverse

osmosis water or a HFD (0.2% cholesterol, high-fat trans-fat with 45% calories from fat; Envigo, Indianapolis, IN) coupled with a high fructose corn syrup equivalent (55% fructose, 45% glucose, w/w) dissolved in reverse osmosis water for 16 wk (20). In all groups, liver and body weight and liver to body weight ratio were measured; serum, total liver, feces, cholangiocytes, hepatocytes and cholangiocyte/hepatocyte supernatants were collected.

Human samples

Liver samples from healthy human (n=4), NAFLD (n=9) and NASH (n=9) were purchased from Sekisui Xeno Tech (Kansas City, KS). Another 5 NASH liver samples were obtained from Dr. Burcin Ekser under the Institutional Review Board (IRB) approved protocol at Indiana University School of Medicine. Patient demographics are listed in Supplemental Table 2. Human serum samples (Control n=24, NAFLD n=10, NASH [stage 1 n=10, stage 2 n=10, stage 3 n=10, stage 4 n=59]) (Supplemental Table 3) were obtained from either Dr. Burcin Ekser under the IRB approved protocol at Indiana University School of Medicine; Dr. Wasim Dar under the protocol HSC-MS-12–0652 approved by UTHealth, McGovern Medical School IRB and Committee for the Protection of Human Subjects in Houston, Texas; or Dr. Niharika Samala under the IRB approved observational study of patients with NAFLD at Indiana University School of Medicine.

Detailed descriptions for other experimental procedures are described in the Supplemental Information.

Statistical analysis

All data are expressed as the mean ± SD. Differences between groups were analyzed by unpaired Student's *t* test when two groups were analyzed and one-way ANOVA when more than two groups were analyzed, followed by an appropriate *post hoc* test. The level of significance was set at $P < 0.05$.

Results

SCT levels and biliary expression of the SCT/SCTR axis increases in patients with NAFLD/NASH and HFD-fed mice

To address the relevance of SCT and SCTR to human NAFLD and NASH, we measured the expression of SCT and SCTR in liver sections from human subjects. NAFLD and NASH samples showed increased biliary SCT and SCTR immunoreactivity compared to control (Figure 1A, Supplementary Figure 1A). Additionally, the mRNA expression of *SCT* and *SCTR* (in total liver samples) and serum SCT levels were higher in NAFLD and NASH compared to control (Figure 1B-C). The biliary immunoreactivity, as well as the mRNA expression of *Sct* and *Sctr* was higher in WT HFD compared to WT CD mice (Figure 1D-E, Supplementary Figure 1B). A very small number of periportal hepatocytes expressing SCTR were observed in liver sections from human NASH (but not NAFLD) and in WT mice fed HFD (Supplementary Figure 1A-B). SCT serum and cholangiocyte supernatant levels were increased in WT HFD compared to WT CD mice (Figure 1F). SCT levels were increased in the supernatant of a human primary cholangiocyte cell line (HIBEpiCs) treated with FFAs (oleate acid (OA), palmitate acid (PA) or stearate acid (SA)) (Supplementary

Figure 1C) along with increased *SCT* and *SCTR* expression (Supplementary Figure 1D) when compared to control.

Knockout of the SCT/SCTR axis protects against HFD-induced liver injury and steatosis

H&E staining demonstrated that, after 16 wk of HFD feeding, WT mice displayed overt NAFLD phenotypes: mixed micro- and macrovesicular steatosis involving 80–90% of hepatocytes; increased portal lymphocytes with interface activity, pericellular fibrosis, increased inflammation with lipogranulomas, and prominent Kupffer cell numbers; these phenotypes were ameliorated in *Sct*$^{-/-}$ and *Sctr*$^{-/-}$ HFD mice (Figure 2A). WT HFD mice had increased serum levels of aspartate aminotransferase (AST), alanine aminotransferase (ALT), and alkaline phosphatase (ALK PHOS) compared to control mice, which were decreased (while AST not significant) in *Sct*$^{-/-}$ and *Sctr*$^{-/-}$ HFD mice compared to WT HFD mice (Supplemental Table 4). Additionally, *Sct*$^{-/-}$ and *Sctr*$^{-/-}$ HFD mice displayed a smaller gain in body weight and lower liver to body weight ratio compared to WT HFD mice (Supplemental Table 4). Furthermore, *Sct*$^{-/-}$ and *Sctr*$^{-/-}$ HFD mice displayed a milder degree of hepatic steatosis compared to WT HFD mice (Figure 2B). The mRNA expression of the fatty acid oxidation genes, *Ppara*, *Acsl1*, and *Cpt1a*, was significantly lower in hepatocytes from WT HFD mice compared to WT CD mice (Figure 2C); however, the expression of these genes was significantly increased in hepatocytes from both *Sct*$^{-/-}$ and *Sctr*$^{-/-}$ HFD mice compared to WT HFD mice (Figure 2C). The mRNA expression of adipogenesis genes *Pparγ*, *Fasn*, and *Acacα* was increased in hepatocytes from WT HFD mice compared to WT CD mice, which was reversed in *Sct*$^{-/-}$ and *Sctr*$^{-/-}$ HFD mice (Figure 2D). Interestingly, the expression of fatty acid oxidation genes was decreased in cholangiocytes from WT HFD mice compared with WT CD mice, but increased in *Sct*$^{-/-}$ and *Sctr*$^{-/-}$ HFD mice (Figure 2E).

SCT/SCTR axis downregulates biliary miR-125b in NAFLD and NASH

Cholangiocyte SCT/SCTR signaling stimulates biliary senescence and liver fibrosis in cholestasis by downregulation of miR-125b (6), and miR-125b may inhibit fat accumulation during HFD (16). We demonstrated that miR-125b expression is much higher in cholangiocytes compared to hepatocytes (Supplementary Figure 2A), and miR-125b expression was decreased in total liver samples from NAFLD and NASH patients compared to control (Figure 3A). In mouse models, the expression of miR-125b was decreased in cholangiocytes from WT HFD mice, which returned to values similar to those of WT CD mice, in *Sct*$^{-/-}$ and *Sctr*$^{-/-}$ HFD mice (Figure 3B). Thus, we aimed to elucidate the mechanisms by which the biliary SCT/SCTR/miR-125b axis (21) regulates hepatocyte lipogenesis. miR-125b mimic and inhibitor were transfected into human hepatocytes (HHs) (Supplementary Figure 2B). miR-125b mimic decreased lipogenesis in transfected HHs treated with FFAs, whereas the miR-125b inhibitor increased lipogenesis (Supplementary Figure 2C). To further explore the paracrine effect of cholangiocyte-derived miR-125b on hepatocyte lipogenesis, we performed TargetScan and KEGG bioinformatic analyses and found 29 lipid biosynthesis genes potentially targeted by miR-125b (Figure 3C). By generating a custom RT^2 Profiler PCR array, we found that 14 of the 29 genes increased in WT HFD mouse hepatocytes compared to WT CD mice, and decreased in *Sct*$^{-/-}$ and *Sctr*$^{-/-}$ HFD mouse hepatocytes compared to WT HFD mice (Figure 3D-E). These 14 genes were further assessed by IPA to identify new and novel targets that have not

previously been published. Our results identified 9 novel genes (*Ifng*, *St8sia4*, *Adh1a3*, *Acer2*, *Pgap3*, *Lpcat4*, *Elovl1*, *St6galnac6*, and *Lclat1*) that are most likely targeted by miR-125b (Supplementary Figure 3A). To verify these observations, *q*PCR was performed to measure the levels of these 9 genes. *Sct*$^{-/-}$ and *Sctr*$^{-/-}$ HFD mice had reduced expression of these genes in hepatocytes compared to WT HFD mice (Figure 3F). These findings identify a novel pathway whereby SCT/SCTR mediates hepatocyte lipogenesis via paracrine miR-125b-dependent signaling.

Downregulation of miR-125b promotes steatosis by upregulating hepatocyte ELOVL1 in NAFLD

We further validated the genes targeted by miR-125b in human NAFLD and NASH, as well as HFD fed mice using TargetScan for both mouse and human sequences, to identify targets with species consistency, and found 5 genes (*Acer2*, *St8sia4*, *St6galnac6*, *Elovl1* and *Lclat1*) from the 9 previously identified for further analysis (Supplementary Figure 3B). Dual luciferase reporter gene assay verified the miR-125b target genes, and the results demonstrated that luciferase signaling was decreased in hepatocytes treated with miR-125b mimic/pmirGLO-Acer2, miR-125b mimic/pmirGLO-Elovl1, miR-125b mimic/pmirGLO-Lclat and miR-125b mimic/pmirGLO-St8sia4 compared with negative control (NC) treatment (Figure 4A). The luciferase activity of the Elovl1 MUT 3'UTR was not significantly different in miR-125b mimic and NC transfected Huh7, indicating that miR-125b specifically binds to *ELOVL1* (Figure 4B). We observed increased mRNA expression of *ELOVL1* in HHs treated with cholangiocyte supernatant from WT HFD mice when compared with supernatant from WT CD mice, which was reduced in HHs treated with cholangiocyte supernatant from *Sct*$^{-/-}$ and *Sctr*$^{-/-}$ HFD mice (Supplementary Figure 3C). Furthermore, ELOVL1 protein expression increased in NAFLD and NASH patients' liver compared with control (Figure 4C). In WT HFD mice, the ELOVL1 expression was increased in hepatocytes compared with WT CD mice; however, knockout of *Sct* or *Sctr* decreased ELOVL1 expression in hepatocytes following HFD feeding (Figure 4E). The immunoreactivity of ELOVL1 was increased in NAFLD and NASH patients compared with control (Figure 4D). There was also enhanced immunoreactivity for ELOVL1 in hepatocytes from WT HFD mice compared with WT CD mice, which was reversed by knockout of *Sct* and *Sctr* (Figure 4F).

Knockout of the SCT/SCTR axis reduces HFD-induced intrahepatic bile duct mass (IBDM) and liver inflammation

By immunohistochemistry (IHC) for CK-19 (co-stained with CD68), IBDM increased in NAFLD samples that did not show a significant increase in CD68 immunoreactivity (Figure 5A), which suggests that IBDM precedes liver inflammation in NAFLD to NASH progression. There was increased IBDM in WT HFD mice compared to WT CD mice, which was reduced in *Sct*$^{-/-}$ and *Sctr*$^{-/-}$ HFD mice (Figure 5B).

Knockout of the SCT/SCTR axis reduces HFD-induced biliary and hepatocyte senescence

SA-β-gal staining demonstrated enhanced biliary and hepatocyte senescence in NAFLD and NASH patients compared to control human samples (Figure 5C). Biliary and hepatocyte senescence increased in WT HFD mice compared to WT CD mice, which was significantly

decreased in *Sct*$^{-/-}$ and *Sctr*$^{-/-}$ HFD mice (Figure 5D, Supplementary Figure 4A). By immunofluorescence, there was enhanced immunoreactivity for p16 in cholangiocytes (co-stained with CK-19) and in hepatocytes (co-stained with HNF4α) from WT HFD mice compared to WT CD (Figure 5E, Supplementary Figure 4B), which decreased in *Sct*$^{-/-}$ and *Sctr*$^{-/-}$ HFD mice. The mRNA expression of the senescence markers, *Cdkn2a*, *Cdkn1a* and *Ccl2*, increased in cholangiocytes from WT HFD mice compared to WT CD, but significantly decreased in *Sct*$^{-/-}$ and *Sctr*$^{-/-}$ HFD mice (Supplementary Figure 4C). *In vitro*, the expression of *Cdkn2c* and *Cdkn1a* increased in immortalized murine cholangiocyte lines (IMCLs) treated with OA, PA or SA compared to control, which was significantly reduced in *Sctr*-shRNA transfected IMCLs (Supplementary Figure 4D).

Knockout of the SCT/SCTR axis decreases HFD-induced liver angiogenesis and inflammation

We next evaluated the expression of (i) VEGF-A (a trophic factor for biliary mitosis and liver fibrosis (17, 21)); and (ii) angiogenic factors that stimulate biliary proliferation and liver fibrosis (22). We demonstrated: (i) enhanced immunoreactivity and mRNA expression for VEGF-A in human NAFLD and NASH compared to control (Figure 6A); (ii) increased expression of vWF in NAFLD and NASH patients compared to control (Figure 6B); and (iii) enhanced VEGF-A immunoreactivity and mRNA expression in WT HFD mice compared to WT CD, which was decreased in *Sct*$^{-/-}$ and *Sctr*$^{-/-}$ HFD mice (Figure 6C). Furthermore, CD31 immunoreactivity and mRNA expression in total liver were significantly higher in WT HFD mice compared with WT CD, but significantly decreased in *Sct*$^{-/-}$ and *Sctr*$^{-/-}$ HFD mice (Figure 6D). Similarly, the mRNA expression of *Vwf* was increased in WT HFD mice compared with WT CD mice but decreased in *Sct*$^{-/-}$ and *Sctr*$^{-/-}$ HFD mice (Supplementary Figure 5A). In addition, there was an increased number of F4/80-positive cells and mRNA expression of *Il1β*, *Il6*, *Il33* and *Tnfα* from WT HFD mice compared with WT CD (Figure 6E, Supplementary Figure 5B), which was decreased in *Sct*$^{-/-}$ and *Sctr*$^{-/-}$ HFD mice.

Knockout of the SCT/SCSR axis reduces HFD-induced liver fibrosis and biliary TGF-β1 levels

There was a significant increase in collagen deposition in WT HFD mice compared to WT CD mice, which was significantly reduced in *Sct*$^{-/-}$ and *Sctr*$^{-/-}$ HFD mice (Figure 7A). The mRNA expression of fibrosis markers increased in total liver samples (Figure 7B) from WT HFD mice compared to WT CD mice, but decreased in *Sct*$^{-/-}$ and *Sctr*$^{-/-}$ HFD mice. Desmin and α-SMA immunoreactivity increased in WT HFD mice compared with WT CD mice (Figure 7C), but this was decreased in *Sct*$^{-/-}$ and *Sctr*$^{-/-}$ HFD mice (Figure 7C). The expression of collagen I was increased in WT HFD mice compared with WT CD mice, but decreased in *Sct*$^{-/-}$ HFD mice (Supplementary Figure 6A). TGF-β1 levels were significantly increased in serum and cholangiocyte supernatants from WT HFD mice compared to WT CD mice but decreased in *Sct*$^{-/-}$ and *Sctr*$^{-/-}$ HFD mice (Figure 7D). Human hepatic stellate cells (HHSteCs) were treated with *in vivo* isolated cholangiocyte supernatants to evaluate the paracrine effect of cholangiocyte-secreted factors (e.g. TGF-β1) on HSC activation. Interestingly, there was increased expression of fibrosis markers (*ACTA2*, *TGF-β1*, *COL1A1* and *FN1*) in HHSteCs treated with cholangiocyte supernatant from WT HFD mice when compared with supernatant from WT CD mice (Supplementary Figure 6B).

However, the fibrosis gene expression was reduced in HHSteCs treated with cholangiocyte supernatant from *Sct*$^{-/-}$ and *Sctr*$^{-/-}$ HFD mice (Figure 7D). Biliary mRNA expression of *Col1a1 Tgf-β1* and *Fn1* was significantly increased in WT HFD mice compared to WT CD mice, but decreased in *Sct*$^{-/-}$ and *Sctr*$^{-/-}$ HFD mice (Supplementary Figure 6C). *In vitro*, the expression of *Col1a1, Tgf-β1 and Fn1* was increased in IMCLs treated with OA, PA or SA compared to control, which was reduced in *Sctr*-shRNA transfected IMCLs (Supplementary Figure 6D).

Knockout of the SCT/SCTR axis alters fecal total bile acid levels, bile acid composition and subsequent signaling pathways

Bile acid data showed that fecal bile acid levels and composition are more prominently altered than the serum or liver bile acid levels and composition in *Sct*/*Sctr* knockout mice compared to WT mice (Supplementary Table 5-10). Of note, *Sct* or *Sctr* knockout increased total bile acid fecal excretion (Supplementary Table 9), but also significantly increased the level of secondary bile acids that are metabolized by the gut microbiota (e.g. ωMCA and DCA), thus demonstrating that *Sct*/*Sctr* knockout may modify the gut microbiota (Supplementary Table 6). While not significant, total bile acid levels were reduced in the liver but enhanced in the serum of *Sct* and *Sctr* knockout mice fed HFD compared to WT HFD mice (Supplementary Table 8, Supplementary Table 10). The expression of ASBT (apical Na+-dependent bile acid transporter, upregulated by secretin) gene, Slc10a2, was increased in cholangiocytes from WT HFD mice compared to WT CD mice, which was reversed in *Sct*$^{-/-}$ or *Sctr*$^{-/-}$ HFD mice (Supplementary Figure 7A), and loss of biliary ASBT may decrease cholehepatic shunting thus leading to the aforementioned changes in hepatic and serum total bile acid levels. Furthermore, the expression of Cyp7b1 was decreased in hepatocytes from WT HFD mice compared to WT CD mice, but was increased in hepatocytes from *Sct*$^{-/-}$ and *Sctr*$^{-/-}$ HFD mice (Supplementary Figure 7B), which may also account for the enhanced serum and fecal bile acid levels.

Discussion

The SCT/SCTR axis exerts pleiotropic effects, including regulation of fluid homeostasis (23) and development of obesity (24). The SCT/SCTR axis, only expressed by cholangiocytes in the liver (25), stimulates ductular reaction/senescence (by an autocrine loop) (21, 26) and liver fibrosis (by a paracrine loop) (5) in cholestasis (4). SCT stimulates lipolysis and lipid absorption in adipose cells (24) and *Sctr* knockout mice are resistant to HFD-induced obesity (9). The liver constitutes an essential organ in lipid metabolism and is a central regulator of lipid homeostasis (27). In this study, we provide data indicating that biliary SCT/SCTR signaling is associated with changes in biliary senescence (by an autocrine loop) and liver steatosis, fibrosis and angiogenesis (by paracrine mechanisms) in NAFLD/NASH. *Sct* or *Sctr* knockout decreases HFD-induced liver steatosis by regulating miR-125b/ELOVL1 expression in hepatocytes. HFD-induced biliary/hepatocyte senescence, DR, liver fibrosis and angiogenesis were reduced by *Sct* or *Sctr* knockout, and *Sct* or *Sctr* knockout increased total bile acid fecal excretion in HFD mice.

In human NAFLD/NASH and HFD-fed mice, we observed increased biliary expression of the SCT/SCTR and enhanced SCT serum levels, providing the first evidence that the SCT/SCTR axis is linked to NAFLD/NASH. Furthermore, *in vitro* cholangiocytes treated with FFAs displayed increased SCT secretion supporting the specific, direct interaction of FFAs with cholangiocytes. Taken together with our previous studies showing that enhanced SCT/SCTR expression induces DR and liver fibrosis in cholestasis (4, 28), our work suggests that enhanced SCT/SCTR signaling regulates the phenotypes (e.g., liver inflammation, steatosis and fibrosis) of NAFLD/NASH.

Although we have previously demonstrated that SCT and SCTR are only expressed by cholangiocytes in control human liver and are upregulated during cholestatic liver injury, we wanted to evaluate if there is a change in hepatocyte SCT and SCTR expression in models of steatosis and steatohepatitis. We observed that a small number of periportal hepatocytes express SCTR in both human NASH and WT mice fed HFD; however, whether these SCTR positive hepatocytes are hepatocytes acquiring biliary phenotypes, or they are cholangiocytes that are transdifferentiating to hepatocytes needs to be further studied.

Hepatic steatosis, defined by triglyceride accumulation in hepatocytes, is the earliest manifestation of NAFLD (29). *Sct* and *Sctr* knockout ameliorated HFD-induced hepatic steatosis. During hepatic lipid homeostasis, *de novo* lipogenesis is instrumental in the development of hepatic steatosis (30). Studies using stable isotope tracers suggest that one important characteristic of NAFLD is abnormally elevated hepatocyte lipogenesis (31). Our data shows that the expression of lipogenesis genes was reversed in $Sct^{-/-}$ or $Sctr^{-/-}$ HFD hepatocytes compared to WT HFD. Studies have shown that miR-125b is also implicated in different liver diseases (32). miR-125b promotes HSC activation by activating RhoA signaling in CCl_4 or BDL mouse models (32). miR-125b promotes the NF-κB-mediated inflammatory response in hepatocytes from NAFLD (33). We have previously demonstrated that SCT/SCTR mediated downregulation of miR-125b promotes biliary proliferation and liver fibrosis during cholestasis (6, 21), whereas overexpression of miR-125b protects HFD-induced hepatic steatosis (16). In our study, miR-125b expression was decreased in human NAFLD/NASH liver and WT HFD mouse cholangiocytes, which was reversed by *Sct* or *Sctr* knockout. In addition, we found the expression of miR-125b is increased in cholangiocytes compared to hepatocytes. Therefore, we propose that SCT-dependent miR-125b plays a role in the modulation of NAFLD phenotypes by paracrine mechanisms. It is known that cell–cell communication is mediated via extracellular vesicle (EV)-delivered miRNAs (34), suggesting a possible paracrine cross-talk between cholangiocytes and hepatocytes likely mediated by SCT/SCTR/miR-125b signaling.

Our data verified that the lipogenesis gene *Elovl1* is a target of miR-125b. ELOVL1 is increased in NASH *Pten* null livers, which increases liver lipogenesis (35). This study identifies that changes in a signaling pathway specific to cholangiocytes (i.e., SCT/SCTR axis) modulate, in a paracrine fashion, hepatic steatosis during NAFLD/NASH. Nevertheless, our studies do not exclude the possibility that SCT effects on hepatic steatosis may be due to impaired intestinal lipid absorption (9), but this issue will be elucidated by feeding cholangiocyte-specific $Sctr^{-/-}$ mice with HFD. Our data herein demonstrates that

miR-125b targets ELOVL1 to regulate hepatocytes lipogenesis, indicating that the biliary SCT/SCTR axis has a direct effect on hepatic steatosis.

SCT-regulated miR-125b targets VEGF-A in models of cholestasis (17), and we noted increased VEGF-A expression and angiogenesis in human NAFLD/NASH. Angiogenesis, defined as new vessel formation from pre-existing vessels, is a key event in NAFLD progression (36) and pathologic angiogenesis increases with NASH (37). VEGF-A expression and angiogenesis were increased in HFD fed mice but reduced with knockout of *Sct* or *Sctr*. These findings suggest that biliary SCT/SCTR/miR-125b axis regulates angiogenesis in NAFLD/NASH. The hepatic inflammatory response is an important driving force of NAFLD progression to NASH (38). We found that depletion of *Sct* or *Sctr* reduced proinflammatory responses in HFD fed mice, demonstrating the paracrine role of the SCT/SCTR axis in regulating inflammatory events during NASH development. Portal inflammatory infiltrate is significantly associated with periportal DR in NAFLD (39), and DR in NAFLD accompanies more advanced histological impairments (8). HFD-induced DR was reduced in $Sct^{-/-}$ or $Sctr^{-/-}$ mice, and other studies have demonstrated that: (i) SCT stimulates biliary proliferation in cholestasis (21); and (ii) knockout of *Sct* or *Sctr*, or treatment of cholestatic rodents with a SCTR antagonist decreases DR (5, 6, 21). We observed DR in human NAFLD samples without significant inflammatory infiltrate, suggesting that DR precedes liver inflammation in NAFLD/NASH. These findings further highlight the paracrine role of the biliary SCT/SCTR axis in NAFLD/NASH development. Aside from DR, senescent cholangiocytes play various roles in aggravated liver inflammation and fibrosis by secreting senescence-associated secretory phenotypes (SASPs) (4, 40, 41). Evidence suggests that senescence is involved cholangiopathy pathogenesis (42), and our lab has shown that $Sctr^{-/-}$ mice have reduced biliary senescence in cholestatic models (5, 6). In this study, cholangiocyte senescence was observed in human NAFLD/NASH (43) and HFD fed mice, but was significantly decreased in $Sct^{-/-}$ or $Sctr^{-/-}$ HFD mice. FFAs can induce cholangiocyte damage in NAFLD (7). Interestingly, our data found that *in vitro* knockdown of cholangiocyte *Sctr* decreased senescence following FFAs treatment, providing further evidence that loss of SCT/SCTR signaling reduces biliary damage during NAFLD progression. One study has demonstrated that hepatocyte senescence correlates closely with fibrosis stage and predicts progression in NAFLD (44). Herein, we found that hepatocyte senescence increased in human NAFLD/NASH and HFD-fed mice, and *Sct* or *Sctr* knockout decreases HFD-induced hepatocyte senescence.

Fibrosis is associated with long-term outcomes in NASH (45), and the presence of advanced fibrosis, including bridging fibrosis and cirrhosis, has the highest risk of mortality related to liver disease (46). In NAFLD/NASH, fibrosis can be followed by steatosis (47), angiogenesis (18), portal inflammation (38) and biliary senescence (48). After HFD feeding, WT mice showed enhanced hepatic fibrosis, which was decreased in $Sct^{-/-}$ or $Sctr^{-/-}$ HFD mice. HSC activation is crucial for the deposition of the extracellular matrix during liver fibrosis, which was observed in HHSteCs treated with cholangiocyte supernatant from WT HFD mice (containing higher levels of TGF-β1), but this was not noted in HHSteCs treated with cholangiocyte supernatant from $Sct^{-/-}$ or $Sctr^{-/-}$ HFD mice (containing little to no TGF-β1). These findings support our hypothesis that biliary SCT/SCTR signaling promotes hepatic fibrosis.

NAFLD and NASH might be linked to dysregulation of cholesterol metabolism through the alternative pathway of bile acid synthesis that is mediated by Cyp7b1 (49). We analyzed the bile acid profile in liver, serum and feces samples in our mice fed CD or HFD. We found that knockout of *Sct* or *Sctr* increases total bile acid fecal excretion and modulates secondary bile acid metabolized by the gut microbiota. Interestingly, the ASBT gene, *Slc10a2*, expression was increased in WT HFD cholangiocytes but decreased in $Sct^{-/-}$ or $Sctr^{-/-}$ HFD mice, showing reduced cholehepatic shunting. We hypothesize that a similar mechanism maybe occurring in the intestines, whereby the increased bile acid fecal excretion may be due to reduced enterohepatic circulation regulated by SCT/ASBT in the intestines, but this warrants further studies. Parallel with previous findings (50), we demonstrated that *Cyp7b1* expression was decreased in WT HFD hepatocytes, whereas *Sct* or *Sctr* knockout reverses the expression of *Cyp7b1*, which indicates *Sct* or *Sctr* knockout alleviate HFD-induced liver injury by altering bile acid pathway.

In conclusion, we have demonstrated that cholangiocytes play a key role in regulating hepatic steatosis during NAFLD. We demonstrate that the biliary SCT/SCTR/miR-125b axis plays an important role in regulating biliary senescence, steatosis, angiogenesis, inflammation, and hepatic fibrosis in NAFLD/NASH (Figure 8). Targeting the biliary SCT/SCTR/miR-125b axis may be key for ameliorating phenotypes of human NAFLD/NASH.

Supplementary Material

Refer to Web version on PubMed Central for supplementary material.

Acknowledgment:

We would like to thank Dr. Naga Chalasani for providing human NAFLD/NASH serum samples under the IRB approved observational study of patients with NAFLD/NASH at Indiana University School of Medicine.

Financial support statement: This work was supported by the Hickam Endowed Chair, Gastroenterology, Medicine (GA), Indiana University, the Indiana University Health – Indiana University School of Medicine Strategic Research Initiative (GA and HF); the VA Merits 5I01BX000574 to GA and 1I01BX003031 to HF from the United States Department of Veteran's Affairs, Biomedical Laboratory Research and Development Service and NIH grants DK108959 and DK119421 (HF), DK076898, DK107310 and DK110035 to GA, and SG. R01 DK121330–01 and R01 DK122796–01 to WD. This material is the result of work supported by resources at the Central Texas Veterans Health Care System, Temple, TX, Richard L. Roudebush VA Medical Center, Indianapolis, IN, and Medical Physiology, Medical Research Building, Temple, TX. The views expressed in this article are those of the authors and do not necessarily represent the views of the Department of Veterans Affairs.

Abbreviations:

ACTA2 (α-SMA)	Actin Alpha 2, Smooth Muscle (α-smooth muscle actin)
Acacα	acetyl-CoA carboxylase alpha
Acer2	Alkaline ceramidase 2
Acsl1	long chain Acyl CoA synthetase
Aldh1a3	Aldehyde dehydrogenase 1 family member A3
CCL2	C-C motif chemokine ligand 2

CD68	cluster of differentiation 68
CK-19	cytokeratin-19
Col1a1	collagen type I alpha 1
Cdkn1a (p21)	cyclin dependent kinase inhibitor 1a
Cdkn2a (p16)	cyclin dependent kinase inhibitor 2a
Cdkn2c (p18)	cyclin dependent kinase inhibitor 2c
Cpt1α	carnitine palmitoyl-transferase 1α
Cyp7b1	oxysterol 7α-hydroxylase
ELOVL1	Elongation of very-long-chain fatty acids 1
ELISA	enzyme linked immunosorbent assay
Fasn	fatty acid synthase
FFAs	free fatty acids
Fn1	fibronectin1
GAPDH	glyceraldehyde-3-phosphate dehydrogenase
HHs	Human hepatocytes
HIBEpiCs	human primary cholangiocyte cell line
HHSteCs	human hepatic stellate cells
HSCs	hepatic stellate cells
IBDM	intrahepatic bile duct mass
Ifnγ	Interferon Gamma
IMCLs	immortalized murine cholangiocyte lines
Lclat1	Lysocardiolipin Acyltransferase 1
LCM	laser capture microdissection
Lpcat4	Lysophosphatidylcholine Acyltransferase 4
NAFLD	nonalcoholic fatty liver disease
NASH	nonalcoholic steatohepatitis
OA	Oleic acid
PA	Palmitic acid
Pecam1 (CD31)	platelet endothelial cell adhesion molecule 1

Pgap3	Post-GPI Attachment To Proteins Phospholipase 3
Pparα	peroxisome proliferator activated receptor α
Pparγ	peroxisome proliferator activated receptor γ
PSC	primary sclerosing cholangitis
SA	Stearate acid
Sct	secretin
Sctr	secretin receptor
St6galnac6	ST6 N-Acetylgalactosaminide Alpha-2,6-Sialyltransferase 6
St8sia4	ST8 Alpha-N-Acetyl-Neuraminide Alpha-2,8-Sialyltransferase 4
Slc10a2 (ASBT)	solute carrier family 10 member 2
TGF-β1	transforming growth factor-β1
VEGF-A	vascular endothelial growth factor-A
vWF	von Willebrand factor
WT	wild-type

REFERENCES

1. Sanyal AJ. Past, present and future perspectives in nonalcoholic fatty liver disease. Nat Rev Gastroenterol Hepatol 2019;16:377–386. [PubMed: 31024089]
2. Ludwig J, Viggiano TR, McGill DB, Oh BJ. Nonalcoholic steatohepatitis: Mayo Clinic experiences with a hitherto unnamed disease. Mayo Clin Proc 1980;55:434–438. [PubMed: 7382552]
3. Estes C, Razavi H, Loomba R, Younossi Z, Sanyal AJ. Modeling the epidemic of nonalcoholic fatty liver disease demonstrates an exponential increase in burden of disease. Hepatology 2018;67:123–133. [PubMed: 28802062]
4. Wu N, Meng F, Invernizzi P, Bernuzzi F, Venter J, Standeford H, Onori P, et al. The secretin/secretin receptor axis modulates liver fibrosis through changes in transforming growth factor-beta1 biliary secretion in mice. Hepatology 2016;64:865–879. [PubMed: 27115285]
5. Wu N, Meng F, Zhou T, Venter J, Giang TK, Kyritsi K, Wu C, et al. The Secretin/Secretin Receptor Axis Modulates Ductular Reaction and Liver Fibrosis through Changes in Transforming Growth Factor-beta1-Mediated Biliary Senescence. Am J Pathol 2018;188:2264–2280. [PubMed: 30036520]
6. Zhou T, Wu N, Meng F, Venter J, Giang TK, Francis H, Kyritsi K, et al. Knockout of secretin receptor reduces biliary damage and liver fibrosis in Mdr2(-/-) mice by diminishing senescence of cholangiocytes. Lab Invest 2018;98:1449–1464. [PubMed: 29977037]
7. Natarajan SK, Ingham SA, Mohr AM, Wehrkamp CJ, Ray A, Roy S, Cazanave SC, et al. Saturated free fatty acids induce cholangiocyte lipoapoptosis. Hepatology 2014;60:1942–1956. [PubMed: 24753158]
8. Sorrentino P, Tarantino G, Perrella A, Micheli P, Perrella O, Conca P. A clinical-morphological study on cholestatic presentation of nonalcoholic fatty liver disease. Dig Dis Sci 2005;50:1130–1135. [PubMed: 15986869]

9. Sekar R, Chow BK. Secretin receptor-knockout mice are resistant to high-fat diet-induced obesity and exhibit impaired intestinal lipid absorption. FASEB J 2014;28:3494–3505. [PubMed: 24769669]
10. Liu Y, Jiang L, Sun C, Ireland N, Shah YM, Liu Y, Rui L. Insulin/Snail1 axis ameliorates fatty liver disease by epigenetically suppressing lipogenesis. Nat Commun 2018;9:2751. [PubMed: 30013137]
11. Smith GI, Shankaran M, Yoshino M, Schweitzer GG, Chondronikola M, Beals JW, Okunade AL, et al. Insulin resistance drives hepatic de novo lipogenesis in nonalcoholic fatty liver disease. J Clin Invest 2020;130:1453–1460. [PubMed: 31805015]
12. Lambert JE, Ramos-Roman MA, Browning JD, Parks EJ. Increased de novo lipogenesis is a distinct characteristic of individuals with nonalcoholic fatty liver disease. Gastroenterology 2014;146:726–735. [PubMed: 24316260]
13. Ohno Y, Suto S, Yamanaka M, Mizutani Y, Mitsutake S, Igarashi Y, Sassa T, et al. ELOVL1 production of C24 acyl-CoAs is linked to C24 sphingolipid synthesis. Proc Natl Acad Sci U S A 2010;107:18439–18444. [PubMed: 20937905]
14. Ambros V. The functions of animal microRNAs. Nature 2004;431:350–355. [PubMed: 15372042]
15. Rottiers V, Naar AM. MicroRNAs in metabolism and metabolic disorders. Nat Rev Mol Cell Biol 2012;13:239–250. [PubMed: 22436747]
16. Zhang ZC, Liu Y, Xiao LL, Li SF, Jiang JH, Zhao Y, Qian SW, et al. Upregulation of miR-125b by estrogen protects against non-alcoholic fatty liver in female mice. J Hepatol 2015;63:1466–1475. [PubMed: 26272872]
17. Kennedy LL, Hargrove LA, Graf AB, Francis TC, Hodges KM, Nguyen QP, Ueno Y, et al. Inhibition of mast cell-derived histamine secretion by cromolyn sodium treatment decreases biliary hyperplasia in cholestatic rodents. Lab Invest 2014;94:1406–1418. [PubMed: 25365204]
18. Hammoutene A, Rautou PE. Role of liver sinusoidal endothelial cells in non-alcoholic fatty liver disease. J Hepatol 2019;70:1278–1291. [PubMed: 30797053]
19. Chu JY, Chung SC, Lam AK, Tam S, Chung SK, Chow BK. Phenotypes developed in secretin receptor-null mice indicated a role for secretin in regulating renal water reabsorption. Mol Cell Biol 2007;27:2499–2511. [PubMed: 17283064]
20. Mells JE, Fu PP, Kumar P, Smith T, Karpen SJ, Anania FA. Saturated fat and cholesterol are critical to inducing murine metabolic syndrome with robust nonalcoholic steatohepatitis. J Nutr Biochem 2015;26:285–292. [PubMed: 25577467]
21. Glaser S, Meng F, Han Y, Onori P, Chow BK, Francis H, Venter J, et al. Secretin stimulates biliary cell proliferation by regulating expression of microRNA 125b and microRNA let7a in mice. Gastroenterology 2014;146:1795–1808 e1712. [PubMed: 24583060]
22. Gaudio E, Barbaro B, Alvaro D, Glaser S, Francis H, Ueno Y, Meininger CJ, et al. Vascular endothelial growth factor stimulates rat cholangiocyte proliferation via an autocrine mechanism. Gastroenterology 2006;130:1270–1282. [PubMed: 16618418]
23. Chu JY, Lee LT, Lai CH, Vaudry H, Chan YS, Yung WH, Chow BK. Secretin as a neurohypophysial factor regulating body water homeostasis. Proc Natl Acad Sci U S A 2009;106:15961–15966. [PubMed: 19805236]
24. Miegueu P, Cianflone K, Richard D, St-Pierre DH. Effect of secretin on preadipocyte, differentiating and mature adipocyte functions. Int J Obes (Lond) 2013;37:366–374. [PubMed: 22565418]
25. Alpini G, Ulrich CD 2nd, Phillips JO, Pham LD, Miller LJ, LaRusso NF. Upregulation of secretin receptor gene expression in rat cholangiocytes after bile duct ligation. Am J Physiol Gastrointest Liver Physiol 1994;266:G922–928.
26. Glaser S, Lam IP, Franchitto A, Gaudio E, Onori P, Chow BK, Wise C, et al. Knockout of secretin receptor reduces large cholangiocyte hyperplasia in mice with extrahepatic cholestasis induced by bile duct ligation. Hepatology 2010;52:204–214. [PubMed: 20578263]
27. Nguyen P, Leray V, Diez M, Serisier S, Le Bloc'h J, Siliart B, Dumon H. Liver lipid metabolism. J Anim Physiol Anim Nutr (Berl) 2008;92:272–283. [PubMed: 18477307]

28. Kennedy L, Francis H, Invernizzi P, Venter J, Wu N, Carbone M, Gershwin ME, et al. Secretin/secretin receptor signaling mediates biliary damage and liver fibrosis in early-stage primary biliary cholangitis. FASEB J 2019;33:10269–10279. [PubMed: 31251081]
29. Ligabue G, Besutti G, Scaglioni R, Stentarelli C, Guaraldi G. MR quantitative biomarkers of non-alcoholic fatty liver disease: technical evolutions and future trends. Quant Imaging Med Surg 2013;3:192–195. [PubMed: 24040614]
30. Ipsen DH, Lykkesfeldt J, Tveden-Nyborg P. Molecular mechanisms of hepatic lipid accumulation in non-alcoholic fatty liver disease. Cell Mol Life Sci 2018;75:3313–3327. [PubMed: 29936596]
31. Diraison F, Moulin P, Beylot M. Contribution of hepatic de novo lipogenesis and reesterification of plasma non esterified fatty acids to plasma triglyceride synthesis during non-alcoholic fatty liver disease. Diabetes Metab 2003;29:478–485. [PubMed: 14631324]
32. You K, Li SY, Gong J, Fang JH, Zhang C, Zhang M, Yuan Y, et al. MicroRNA-125b Promotes Hepatic Stellate Cell Activation and Liver Fibrosis by Activating RhoA Signaling. Mol Ther Nucleic Acids 2018;12:57–66. [PubMed: 30195793]
33. Zhang Q, Yu K, Cao Y, Luo Y, Liu Y, Zhao C. miR-125b promotes the NF-kappaB-mediated inflammatory response in NAFLD via directly targeting TNFAIP3. Life Sci 2021;270:119071. [PubMed: 33515562]
34. Valadi H, Ekstrom K, Bossios A, Sjostrand M, Lee JJ, Lotvall JO. Exosome-mediated transfer of mRNAs and microRNAs is a novel mechanism of genetic exchange between cells. Nat Cell Biol 2007;9:654–659. [PubMed: 17486113]
35. Muir K, Hazim A, He Y, Peyressatre M, Kim DY, Song X, Beretta L. Proteomic and lipidomic signatures of lipid metabolism in NASH-associated hepatocellular carcinoma. Cancer Res 2013;73:4722–4731. [PubMed: 23749645]
36. Iwakiri Y, Shah V, Rockey DC. Vascular pathobiology in chronic liver disease and cirrhosis - current status and future directions. J Hepatol 2014;61:912–924. [PubMed: 24911462]
37. Tamaki Y, Nakade Y, Yamauchi T, Makino Y, Yokohama S, Okada M, Aso K, et al. Angiotensin II type 1 receptor antagonist prevents hepatic carcinoma in rats with nonalcoholic steatohepatitis. J Gastroenterol 2013;48:491–503. [PubMed: 22886508]
38. Schuster S, Cabrera D, Arrese M, Feldstein AE. Triggering and resolution of inflammation in NASH. Nat Rev Gastroenterol Hepatol 2018;15:349–364. [PubMed: 29740166]
39. Gadd VL, Skoien R, Powell EE, Fagan KJ, Winterford C, Horsfall L, Irvine K, et al. The portal inflammatory infiltrate and ductular reaction in human nonalcoholic fatty liver disease. Hepatology 2014;59:1393–1405. [PubMed: 24254368]
40. Sasaki M, Miyakoshi M, Sato Y, Nakanuma Y. Chemokine-chemokine receptor CCL2-CCR2 and CX3CL1-CX3CR1 axis may play a role in the aggravated inflammation in primary biliary cirrhosis. Dig Dis Sci 2014;59:358–364. [PubMed: 24185682]
41. Wan Y, Meng F, Wu N, Zhou T, Venter J, Francis H, Kennedy L, et al. Substance P increases liver fibrosis by differential changes in senescence of cholangiocytes and hepatic stellate cells. Hepatology 2017;66:528–541. [PubMed: 28256736]
42. Nakanuma Y, Sasaki M, Harada K. Autophagy and senescence in fibrosing cholangiopathies. J Hepatol 2015;62:934–945. [PubMed: 25435435]
43. Kennedy L, Hargrove L, Demieville J, Bailey JM, Dar W, Polireddy K, Chen Q, et al. Knockout of l-Histidine Decarboxylase Prevents Cholangiocyte Damage and Hepatic Fibrosis in Mice Subjected to High-Fat Diet Feeding via Disrupted Histamine/Leptin Signaling. Am J Pathol 2018;188:600–615. [PubMed: 29248461]
44. Aravinthan A, Scarpini C, Tachtatzis P, Verma S, Penrhyn-Lowe S, Harvey R, Davies SE, et al. Hepatocyte senescence predicts progression in non-alcohol-related fatty liver disease. J Hepatol 2013;58:549–556. [PubMed: 23142622]
45. Loomba R, Chalasani N. The Hierarchical Model of NAFLD: Prognostic Significance of Histologic Features in NASH. Gastroenterology 2015;149:278–281. [PubMed: 26116800]
46. Chalasani N, Younossi Z, Lavine JE, Charlton M, Cusi K, Rinella M, Harrison SA, et al. The diagnosis and management of nonalcoholic fatty liver disease: Practice guidance from the American Association for the Study of Liver Diseases. Hepatology 2018;67:328–357. [PubMed: 28714183]

47. McPherson S, Hardy T, Henderson E, Burt AD, Day CP, Anstee QM. Evidence of NAFLD progression from steatosis to fibrosing-steatohepatitis using paired biopsies: implications for prognosis and clinical management. J Hepatol 2015;62:1148–1155. [PubMed: 25477264]

48. Chiba M, Sasaki M, Kitamura S, Ikeda H, Sato Y, Nakanuma Y. Participation of bile ductular cells in the pathological progression of non-alcoholic fatty liver disease. J Clin Pathol 2011;64:564–570. [PubMed: 21486894]

49. Pandak WM, Kakiyama G. The acidic pathway of bile acid synthesis: Not just an alternative pathway. Liver Res 2019;3:88–98. [PubMed: 32015930]

50. Kakiyama G, Marques D, Martin R, Takei H, Rodriguez-Agudo D, LaSalle SA, Hashiguchi T, et al. Insulin resistance dysregulates CYP7B1 leading to oxysterol accumulation: a pathway for NAFL to NASH transition. J Lipid Res 2020;61:1629–1644. [PubMed: 33008924]

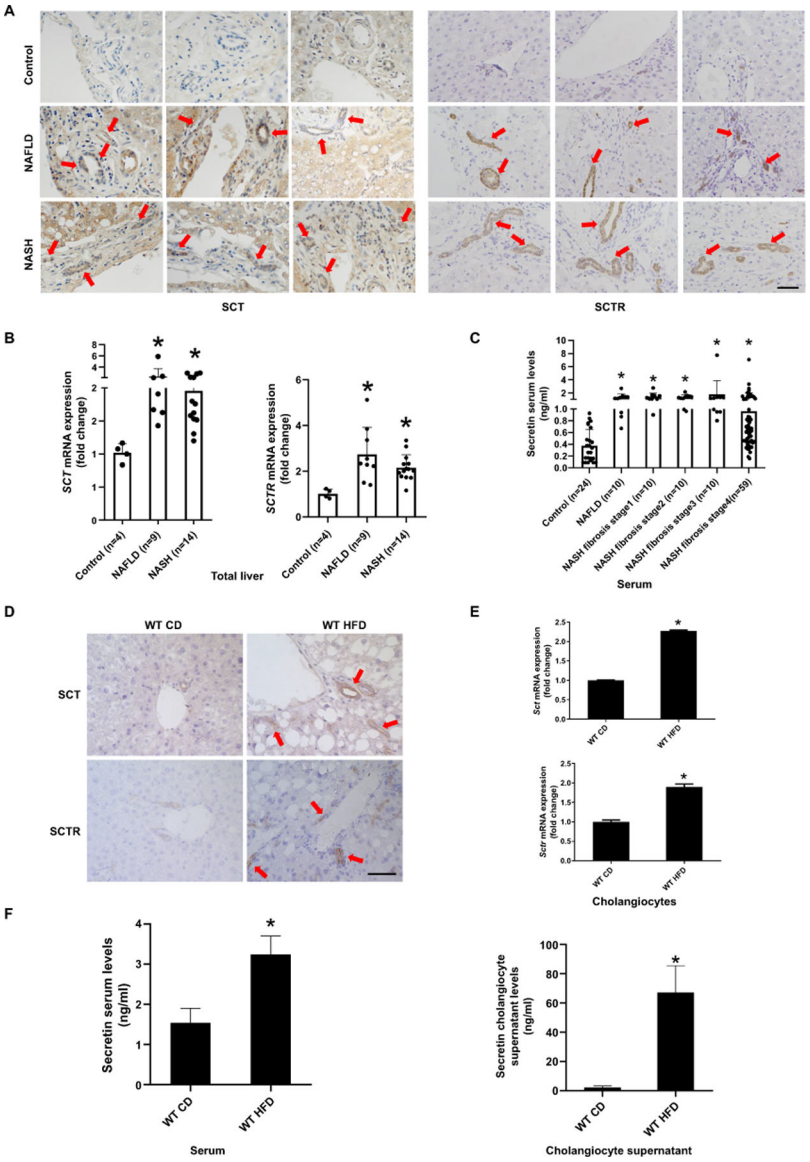

Figure 1. Biliary SCT/SCTR expression is increased in human NAFLD and HFD mice.

(A) Representative IHC images for SCT and SCTR in liver from patients with NAFLD (n=9) and NASH (n=14) and control (n=4) (40×; scale bar, 25 μm). (B) mRNA expression of *SCT* and *SCTR* in human NAFLD (n=9) and NASH (n=15) liver. (C) SCT levels in NAFLD (n=10) and NASH (stage 1–4; n=89) patients' serum. (D) Representative images of SCT and SCTR expression in liver sections from WT CD and WT HFD mice (n=3; 40×; scale bar, 25 μm), E) mRNA expression of *Sct* and *Sctr* in isolated mouse cholangiocytes (n=3 reactions from samples obtained from a cumulative cell preparation from 8 mice). (F) SCT levels in mouse serum and cholangiocyte supernatant (n=3 reactions from samples obtained from a cumulative cell preparation from 8 mice). Data are mean ± SD. **P* <0.05 versus Control or WT CD.

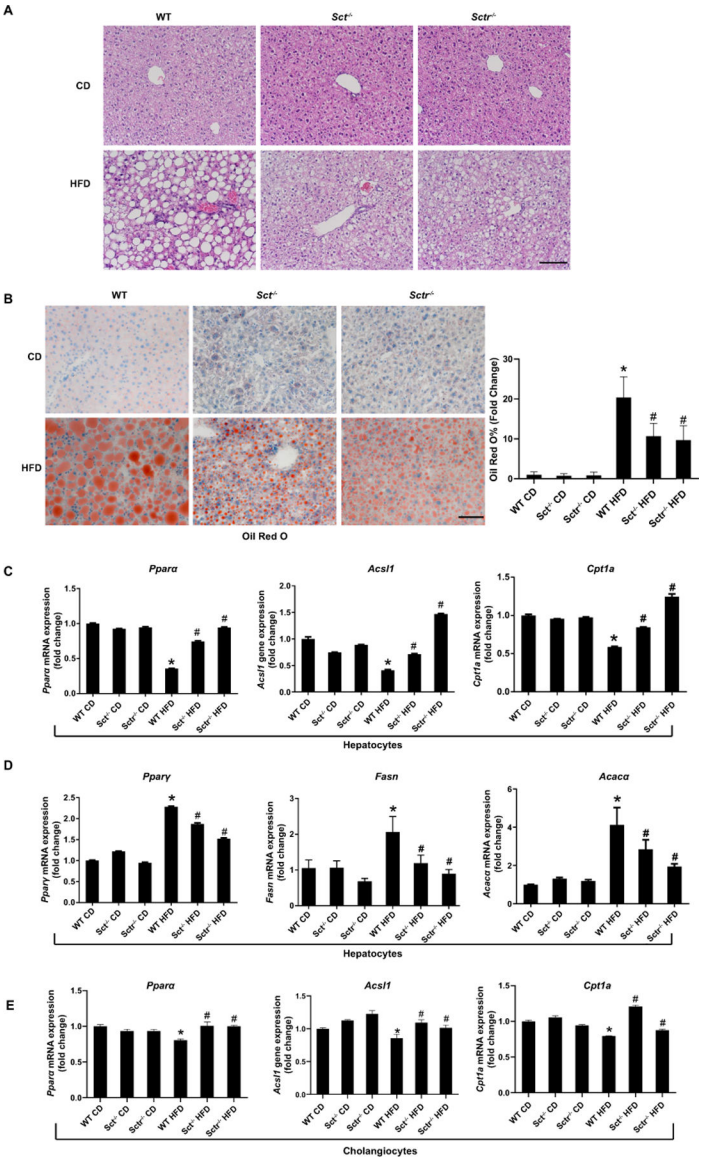

Figure 2. SCT or SCTR knockout protects against HFD-induced steatosis.

(A) Representative H&E images in liver from *Sct*$^{-/-}$ and *Sctr*$^{-/-}$ HFD mice (n=8; 20×; scale bar, 50 μm). (B) Representative images of Oil Red O staining in *Sct*$^{-/-}$ and *Sctr*$^{-/-}$ HFD mice. (n=24 from 8 different mice; 20×; scale bar, 50 μm). (C) Fatty acid oxidation genes *Pparα*, *Acsl1* and *Cpt1α* expression in hepatocytes from *Sct*$^{-/-}$ and *Sctr*$^{-/-}$ HFD mice (n=3 reactions from samples obtained from a cumulative cell preparation from 8 mice). (D) The expression of adipogenesis gene *Pparγ*, *Fasn* and *Acacα* in hepatocytes from *Sct*$^{-/-}$ and *Sctr*$^{-/-}$ HFD mice (n=3 reactions from samples obtained from a cumulative cell preparation from 8 mice). (E) The expression fatty acid oxidation gene (*Pparα*, *Acsl1* and *Cpt1α*) expression in cholangiocytes from *Sct*$^{-/-}$ and *Sctr*$^{-/-}$ HFD mice (n=3 reactions from samples obtained from a cumulative cell preparation from 8 mice). Data are mean ± SD. **P* <0.05 versus WT CD, $^{\#}$*P* <0.05 versus WT HFD.

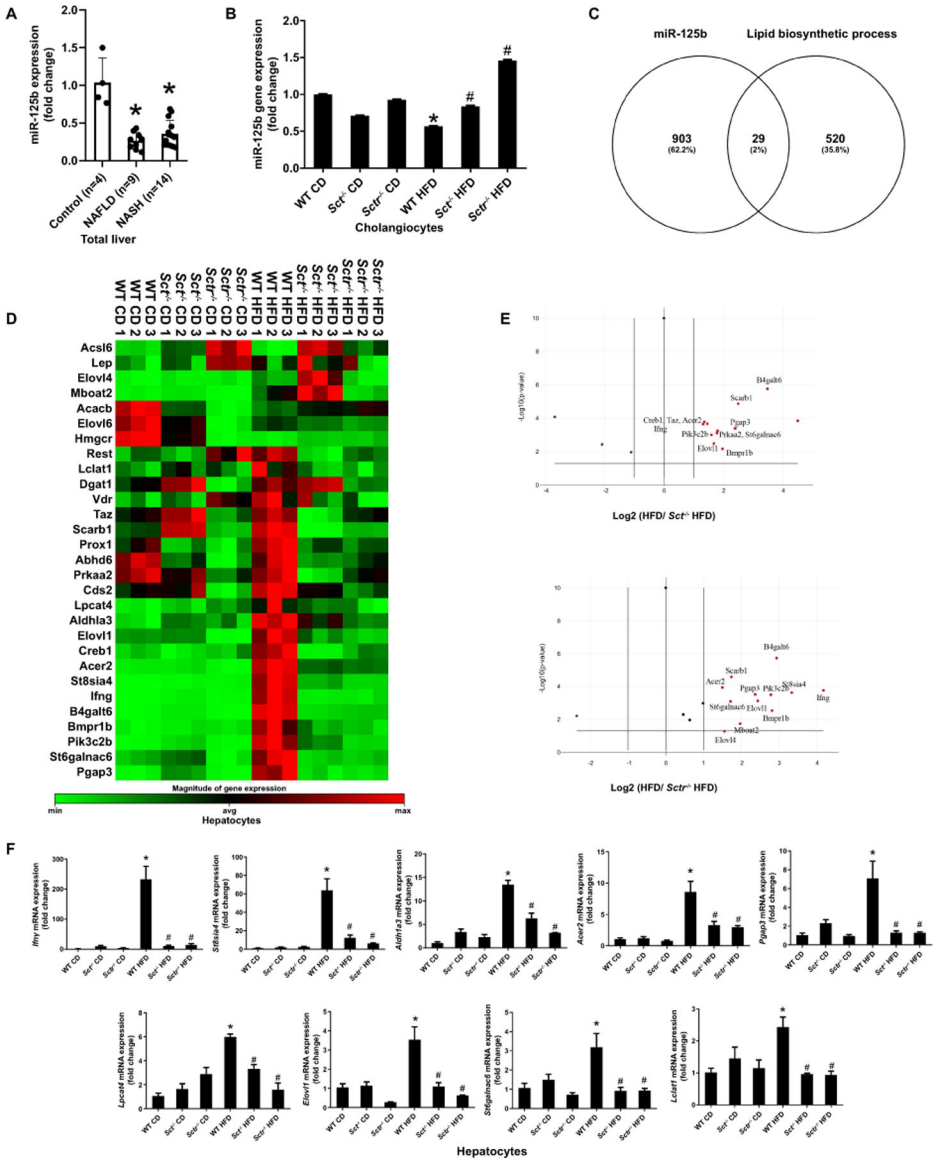

Figure 3. SCT/SCTR axis downregulates biliary miR-125b that targets lipogenesis genes in NAFLD.

(A) miR-125b expression in liver of NAFLD (n=9) and NASH (n=14). (B) miR-125b expression in cholangiocytes from selected mouse groups (n=3 reactions from samples obtained from a cumulative cell preparation from 8 mice). (C) Venn map of predicted miR-125b target lipid biosynthetic process genes by TargetScan and KEGG. (D) Custom RT^2 Profiler PCR array was used to analyze miR-125b potential target lipid biosynthetic process genes expression between WT HFD and *Sct*$^{-/-}$/*Sctr*$^{-/-}$ HFD mouse in hepatocytes (n=3 reactions from samples obtained from a cumulative cell preparation from 8 mice). (E) The Volcano Plot identifies significant gene expression changes. (F) The expression of *Ifng*, *St8sia4*, *Adh1a3*, *Acer2*, *Pgap3*, *Lpcat4*, *Elovl1*, *St6galnac6* and *Lclat1* in mouse hepatocytes (n=3 reactions from samples obtained from a cumulative cell preparation from 8 mice). Data are mean ± SD. **P* <0.05 versus Control or WT CD; #*P* <0.05 versus WT HFD.

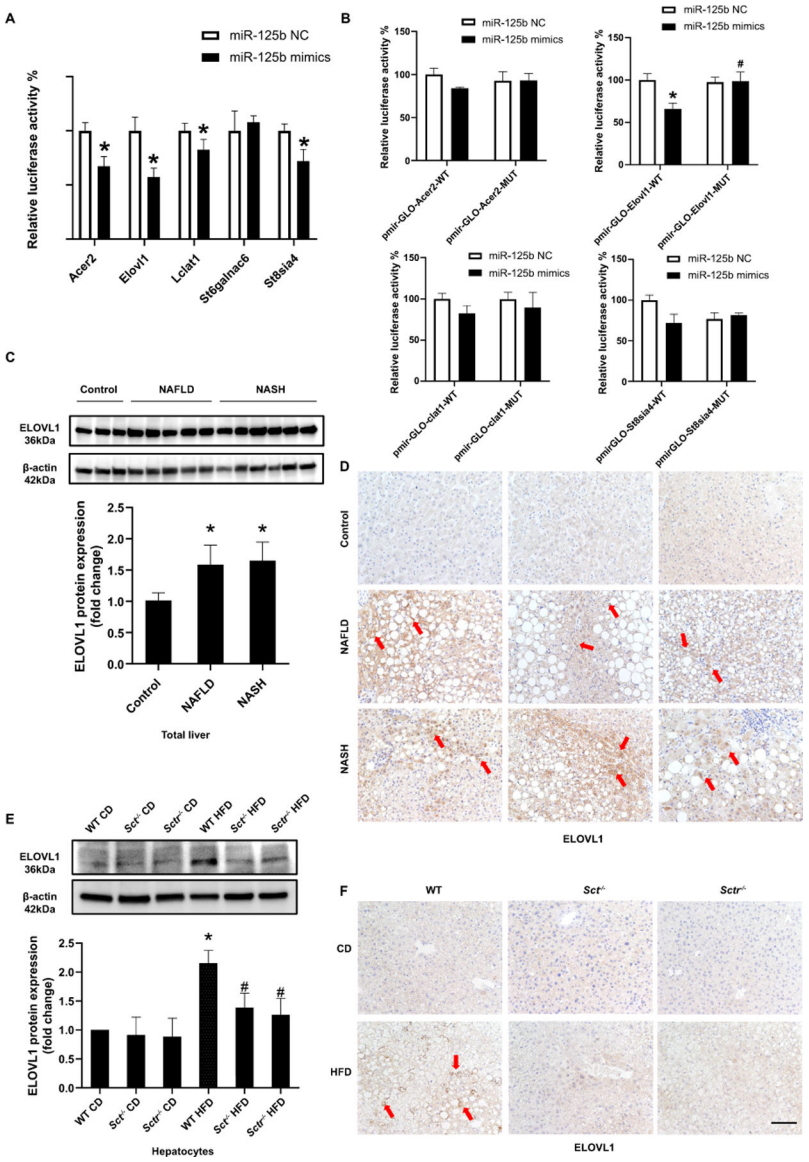

Figure 4. miR-125b promotes steatosis by upregulating Elovl1.

(A) Luciferase activities were detected after post-transfection of pmirGLO vectors (Acer2, St8sia4, St6galnac6, Elovl1 and Lclat1) and miR-125b mimic transfection in Huh7 cells (n=3). (B) Luciferase activities were detected after post-transfection of pmirGLO vectors (Acer2, St8sia4, Elovl1 and Lclat1 MUT 3'UTR) and miR-125b mimic transfection in Huh7 cells (n=3). (C) ELOVL1 expression in NAFLD (n=9) and NASH (n=14) patients (n=4) was detected by western blot. (D) Representative IHC images for ELOVL1 in liver from patients with NAFLD (n=9) and NASH (n=14) and control (n=4) (20×; scale bar, 50 μm). (E) ELOVL1 expression was detected by western blot in mouse isolated hepatocytes (n=3 reactions from samples obtained from a cumulative cell preparation from 8 mice). (F) Representative IHC images for ELOVL1 in mouse livers (n=8; 20×; scale bar, 50 μm). Data are mean ± SD. *P<0.05 versus Control, WT CD or mimic negative control; #P<0.05 versus WT HFD.

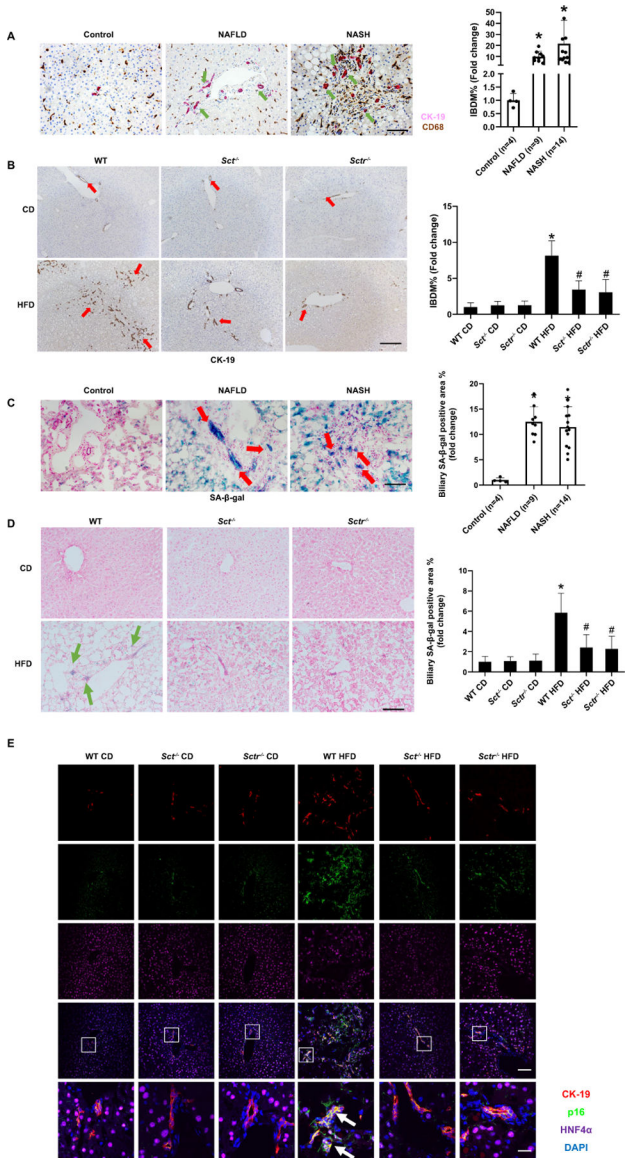

Figure 5. HFD-induced intrahepatic bile duct mass (IBDM) precedes inflammation and is reduced by SCT and SCTR knockout.

(A) Representative IHC images for CK-19 in liver from patients with NAFLD (n=9) and NASH (n=14) and control (n=4) (10×; scale bar, 100 μm)). (B) Representative IHC images for CK-19 in liver from *Sct*$^{-/-}$ and *Sctr*$^{-/-}$ HFD mice (n=24 from 8 different mice; 10×; scale bar, 100 μm). (C) Biliary senescence in liver from NAFLD (n=9) and NASH (n=14) patients was measured by SA-β-gal staining (20×; scale bar, 50 μm). (D) Measurement of biliary senescence in *Sct*$^{-/-}$ and *Sctr*$^{-/-}$ HFD mouse liver by SA-β-gal staining (n=24 from 8 different mice; 20×; scale bar, 50 μm). (E) Immunofluorescence for p16 /CK-19 in *Sct*$^{-/-}$ and *Sctr*$^{-/-}$ HFD mouse livers (n=8; upper four panels: Orig. magn. ×20, scale bar 50 μm; lower panel: Orig. magn. ×100, scale bar 10 μm; red CK-19, green p16, purple HNF4α, blue DAPI; white arrow: p16 positive cholangiocytes). Data are mean ± SD. **P* <0.05 versus Control or WT CD; $^{\#}P$ <0.05 versus WT HFD.

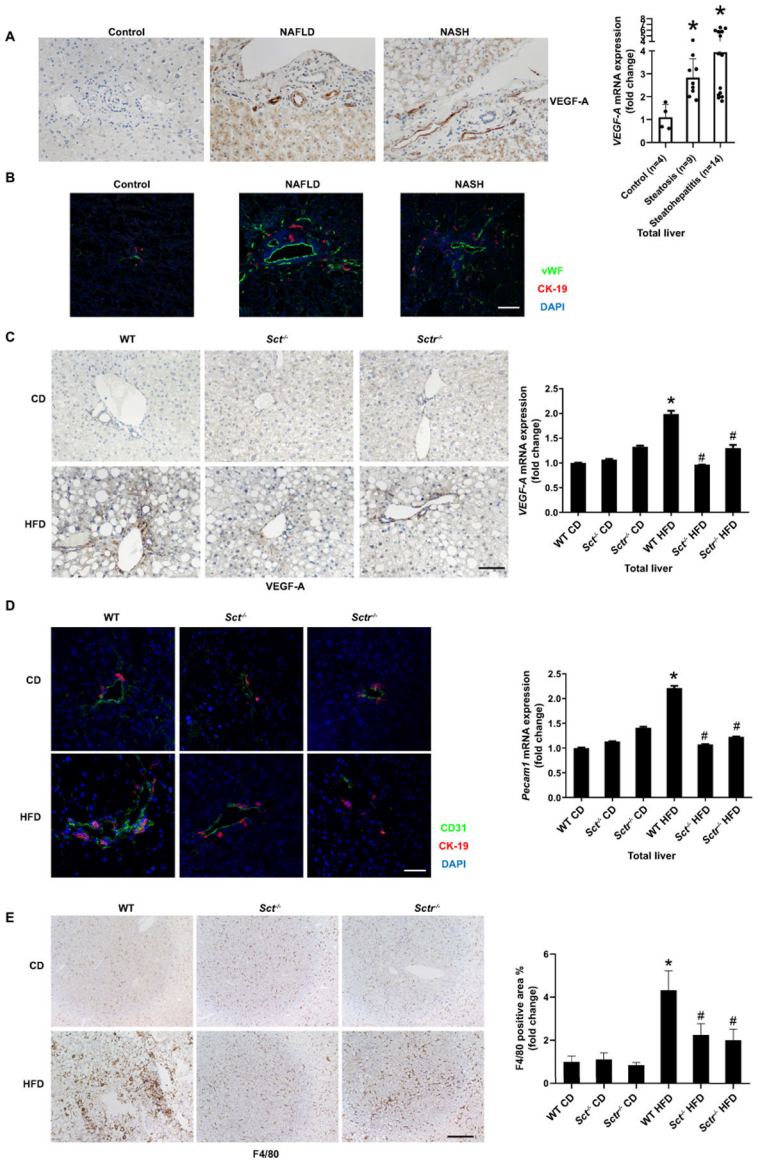

Figure 6. Knockout of the SCT/SCTR decreases HFD-induced liver angiogenesis and inflammation.

(A) VEGF-A expression in livers from NAFLD (n=9) and NASH (n=14) was measured by immunohistochemistry (20×; scale bar, 50 μm) and by *q*PCR. (B) Liver angiogenesis in liver samples from NAFLD (n=9) and NASH (n=14) was observed by immunofluorescence of vWF (20×; scale bar, 50 μm). (C) VEGF-A expression in *Sct*$^{-/-}$ and *Sctr*$^{-/-}$ HFD mouse liver was measured by immunohistochemistry (n=3; 20×; scale bar, 50 μm) and *q*PCR. (D) Angiogenesis in mouse liver samples was observed by immunofluorescence of CD31 (n=3; 40×; scale bar, 25 μm) and *q*PCR of *Pecam1* in total liver (n=3). (E) Liver inflammation was detected by immunohistochemistry for F4/80 in *Sct*$^{-/-}$ and *Sctr*$^{-/-}$ HFD mice (n=24 from 8 different mice; 10×; scale bar, 100 μm). Data are mean ± SD. **P* <0.05 versus WT CD or Control, $^{\#}$*P* <0.05 versus WT HFD.

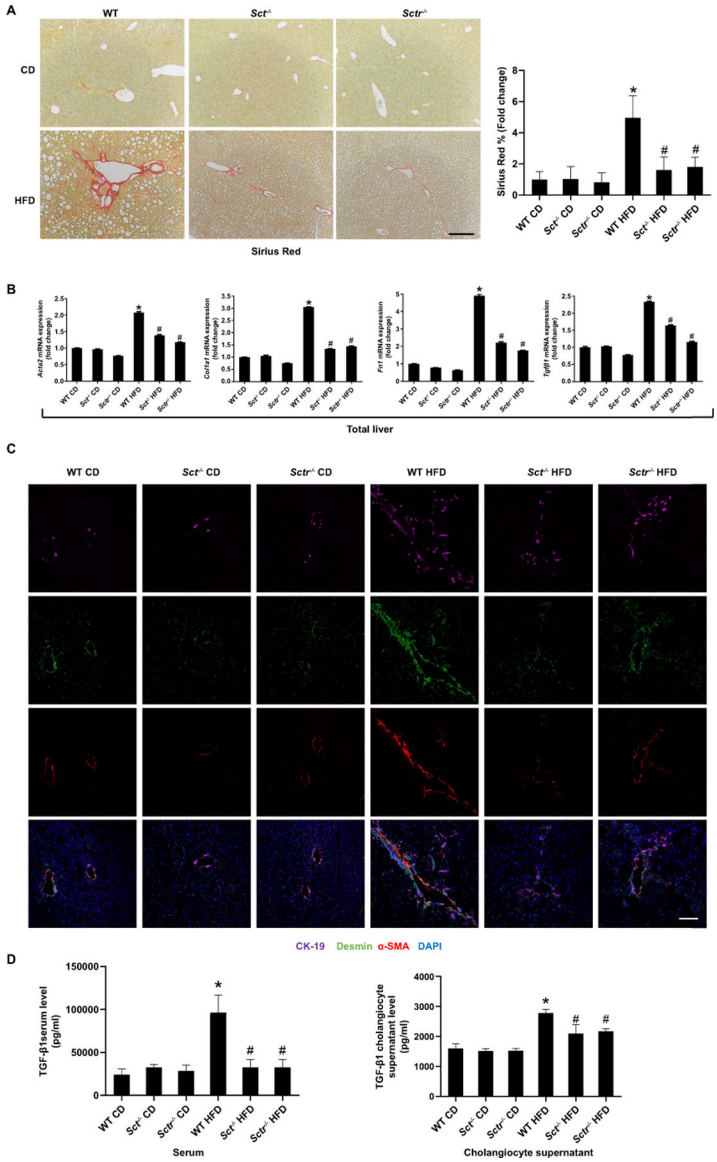

Figure 7. Knockout of the SCT/SCTR axis reduces HFD induced liver fibrosis.

(A) Measurement of collagen deposition by Sirius Red staining in *Sct*$^{-/-}$ and *Sctr*$^{-/-}$ HFD mice liver (n=24 from 8 different mice; 10×; scale bar, 100 μm). (B) mRNA expression of fibrotic markers in *Sct*$^{-/-}$ and *Sctr*$^{-/-}$ HFD mouse total liver; n=3. (C) Immunofluorescence for α-SMA/desmin in mouse livers (n=8; 20×; scale bar, 50 μm). (D) TGF-β1 levels in mouse serum and cholangiocyte supernatant (n=3 reactions from samples obtained from a cumulative cell preparation from 8 mice). Data are mean ± SD. **P* <0.05 versus WT CD, #*P* <0.05 versus WT HFD.

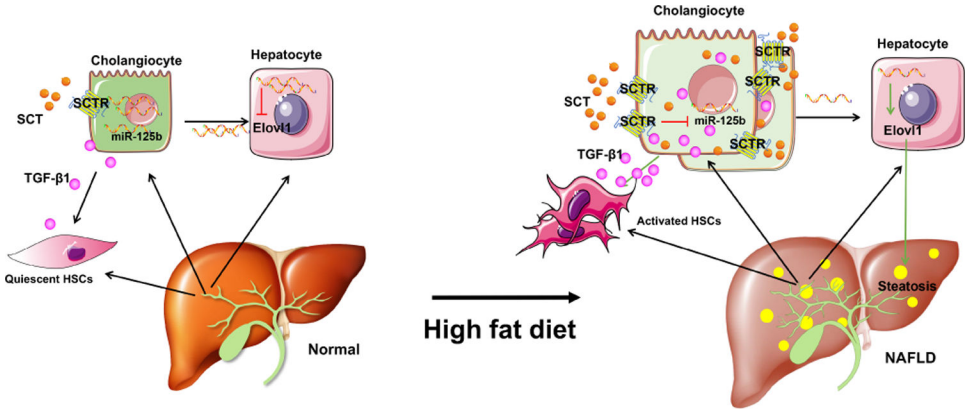

Figure 8. Working model of biliary SCT/SCTR/miR-125b axis regulation of biliary damage, steatosis, and hepatic fibrosis in NAFLD/NASH.

Biliary SCT and SCTR expression is increased in NAFLD. SCT/SCTR downregulation biliary miR-125b promotes steatosis by targeting lipogenesis gene ELOVL1 in NAFLD. Increased cholangiocyte-derived TGF-β1 induces HSC activation by paracrine in NAFLD.